Rapid #: -11626432

CROSS REF ID: **1364777**

LENDER: **AZN :: Main Library**

BORROWER: **UUM :: Marriott Library**

TYPE:	Article CC:CCL
JOURNAL TITLE:	Optical review
USER JOURNAL TITLE:	Optical Review
ARTICLE TITLE:	Applications of Liquid Crystals to Variable-Focusing Lenses
ARTICLE AUTHOR:	S. Sato
VOLUME:	6
ISSUE:	6
MONTH:	
YEAR:	1999
PAGES:	471–485
ISSN:	1340-6000
OCLC #:	

Processed by RapidX: 3/6/2017 11:23:50 AM

OPTICAL REVIEW Vol. 6, No. 6 (1999) 471–485

Review

Applications of Liquid Crystals to Variable-Focusing Lenses

Susumu SATO

Department of Electrical and Electronic Engineering, Akita University, 1-1, Tegata Gakuen-machi, Akita, 010-8502 Japan

(Received August 2, 1999; Accepted September 13, 1999)

Liquid Crystal (LC) lens cells with variable focusing properties are fabricated using nematic LC materials and applicable to optical devices, and our recent work on these cells is described. First, the LC lens cells are prepared using lens-shaped substrates coated with transparent electrodes. Their focal length can be continuously varied between the values for an ordinary ray and an extraordinary ray by changing the voltage passing across them. Methods of improving properties and some applications of the lens-shaped LC lens are briefly described. The lens properties of these cells with plane-paralleled structure are then demonstrated, where the refractive index is graded to a quadratic distribution resulting from an axially symmetric non-uniform electric field. LC cells with axially distributed tilt angles are constructed using a pair of circular hole-patterned electrode substrates and very small LC lens (LC microlens) with variable focusing can be fabricated. Optimizing the electrode structure, device parameters, and material parameters of the LCs, excellent focusing properties can be obtained. The properties of the LC microlens are improved by using the polymer stabilization technique. The LC microlens with a divided electrode structure shows three-dimensional beam steering and focusing properties, and the astigmatic aberration caused by the molecular orientation effect can be compensated. Applications of the LC microlens to optical devices and systems are introduced.

Key words: nematic liquid crystal, liquid crystal lens, microlens, variable focusing, free-space beam steering

1. Introduction

It is well known that nematic liquid crystal (LC) flows and takes the shape of its container like a liquid; that is, positional order is lost, but it still possesses orientational order and anisotropic physical properties similar to crystalline solid.[1] The nematic LC cells in which molecules are uniformly aligned along their long axes parallel to the substrate surface in the same direction, (a homogeneous orientation state), have optical properties similar to those of uniaxial crystals. The direction of long axes of molecules, which is called the director of the LC, can easily be controlled by surface treatment of the substrates; the optical properties of the LC cells can be changed by applying a relatively low electric field across the cells. Many applications for LC cells as flat-panel type display devices with low driving voltage and power consumption have been extensively investigated. In addition to display devices, some applications of LCs to optical devices such as optical waveguides[2,3] and light deflection devices[4,5] were reported, and new optical devices can be produced using LC materials.[6–8]

In most conventional LC display devices using nematic LCs, the LC director is reoriented by a uniform electric field produced by a pair of plane-paralleled electrode structures. Using cells of which the electrode is not a plane-paralleled structure but is a curved, lens-shaped can reorient the LC director. This lens-shaped LC cell becomes a lens by which rays of light are made to converge or diverge, and varying the applied voltage across the lens-cell causes continuous variation in its focal length between the values for an ordinary ray and an extraordinary ray.[6]

Using the plane-paralleled structure where the refractive index is graded to have a quadratic distribution can also attain these properties. The LC director can be reoriented by a non-uniform electric field produced by a hole-patterned electrode structure.[9] In this LC cell, an axially symmetric non-uniform electric field is produced and a radially graded distribution of refractive indices can be observed with a low voltage across the cell. This LC cell is expected to have a lens effect of which the focal length can be controlled by the applied voltage.[9]

In this paper, variable focusing properties of lens-shaped LC cells are described, and methods to improve their drawbacks such as slow response properties, low transmittance and nonlinear driving properties are demonstrated. Next, basic phenomena of the director orientation effects in the axially symmetric nonuniform electric field produced by a circular hole-patterned electrode structure are described, and fabrication and fundamental properties of the LC microlens are briefly reviewed. Optimizing the electrode structure and material parameters, excellent lens properties can be obtained. Improvement in response and optical properties is then described, and introduction of the divided electrode structure, which can also compensate the aberration, can provide free space focusing and deflection properties. The response and recovery time can be greatly reduced by the polymer stabilization technique using UV curable LC materials. Some applications of the lens-shaped LC lens and the LC microlens are offered.

E-mail: satosu@ipc.akita-u.ac.jp

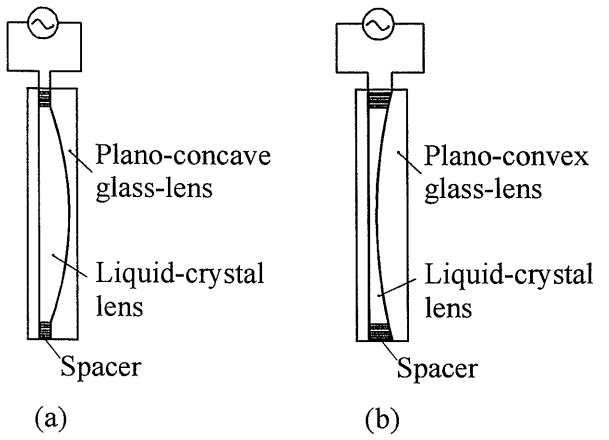

Fig. 1. Structure of the LC lenses showing lens shape. (a) plano-convex LC lens, (b) plano-concave LC lens.

2. LC Lens with Lens-Shape

2.1 Variable Focusing Properties of Homogeneously Aligned LC Lens Cell

Homogeneously aligned LC cells shaped like a plano-convex lens and a plano-concave lens as shown in Fig. 1 (a) and (b) were made using nematic LCs with positive dielectric anisotropy.[6] The LC materials were put into cells fabricated from a transparent electrode coated glass substrate, a spacer of suitable thickness, and a concave or a convex glass lens coated with a transparent electrode. Both electrode surfaces were coated with polyvinylalchohol (PVA) film and rubbed unidirectionally. They show focusing and diverging lens properties; that is, the focal length can be varied continuously between those of f_e and f_o determined by the refractive indices for the extraordinary ray n_e and for the ordinary ray n_o of LC materials, respectively.

2.2 Improvements in Lens Properties by the Fresnel Structure

The thickness of the LC layer becomes extremely large at the center region of a convex lens-cell or at the peripheral part of a concave lens-cell, however, in comparison with that of a usual conventional LC display. This makes the response and recovery properties in this LC lens when applying and removing the driving voltage very slow. In addition, the transmission of incoming light is reduced according to the increase in thickness of the LC layer due to the absorption and/or scattering effect. These properties are disadvantageous for practical use of this type of LC lens but can be improved by decreasing the effective thickness of the LC layers, that is, by adopting the LC layer as the Fresnel structure.[10] For example, for the typical plano-convex LC lens with a diameter of 20 mm and a focal length of 200 mm, the thickness of the LC layer at the center of the cell is about 500 μm. Since the response and recovery times increase as a function of the square of this layer, an improvement of more than two orders of magnitude can be achieved in the same size cells by adopting the LC layer as the Fresnel structure, if

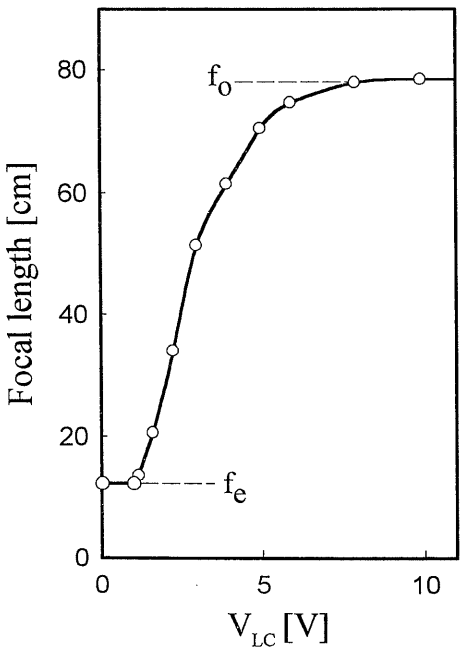

Fig. 2. Relationship between focal length lens and applied voltage across the LC lens.

the groove depth of the Fresnel lens is within about 50 μm. Steep reduction of the response and recovery properties of less than one second and more transparent than 90% for the visible range are the possible.[10] Figure 2 shows the relationship between the applied voltage and the focal length in the LC lens.

Figures 3 (a) and (b) show photographs of imaging properties observed through the Fresnel-type LC lens with and without applied voltage.[11] However, a polarizer is indispensable for the LC lens, since the polarization of the incident light has to be parallel to the rubbing direction of the LC cell; that is, only the component of an extraordinary ray can be effective for variable-focusing properties. Transmittance of the polarizer is usually about 40% or less, so it is hard to make a lens with high transmittance in this system. More transparent variable focusing lenses without polarizers are achieved by combining two identical LC lenses with a mutually orthogonal optic axis.[10]

Since the LC cell has an anisotropy intrinsically due to its molecular orientation, that is the unidirectional orientation of the director, the homogeneously aligned LC lens has a characteristic aberration that does not occur in the conventional glass lens. The effective refractive index of the LC lens where the director is aligned parallel to the grooves of the Fresnel structure is larger than one in which the director is aligned perpendicular to the grooves.[12] In consequence, the focusing properties of the lens differ according to the incidence of the rays on different parts of the lens. The properties of the LC lens can be improved by making the director orientation axially symmetric, in the form of a concentrically circular orientation.[12]

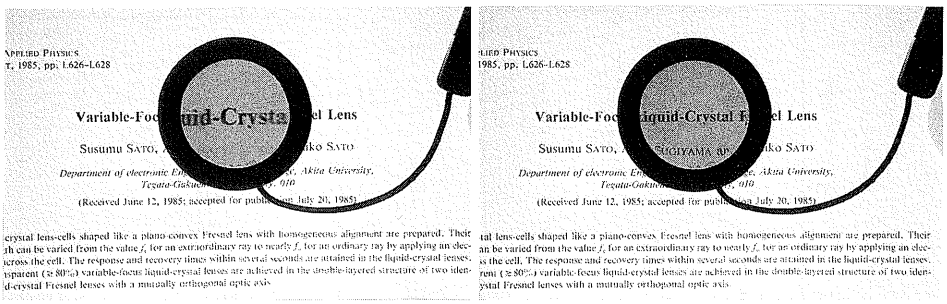

(a) (b)

Fig. 3. Images through the Fresnel-type LC lens. (a) off-state, (b) on-state.

2.3 *Compensation for Nonlinear Properties in a LC Lens*

In the LC lens with a lens-shaped structure, as seen in Fig. 2, the focal length can be continuously varied according to the applied voltage level, and an electrically controllable focusing lens with no mechanical parts can be obtained. However, it is seen from Fig. 2 that the focal length begins to increase at the threshold voltage and saturates gradually as the applied voltage increases. The nonlinear properties between the focal length and applied voltage are great disadvantages for application of the LC lens to various systems. In this section, a method of linearizing the lens properties is described, that is, the driving voltage to compensate the nonlinearity of the lens.

The compensation method for the LC lens is that the lens is driven by the compensation driving voltage,[13] which has an inverse functional property to that shown in Fig. 2. The voltage dependence of the capacitance in the homogeneously aligned LC cell or that of light transmission properties in the guest-host LC cell has similar voltage dependence on the focal length in the LC lens.[13,14]

A block diagram to produce the inverse function of the voltage-transmission properties using the guest-host cell is shown in Fig. 4 (a).[14] An oscillating circuit of 1 kHz with variable amplification was used to drive the guest-host cell. The light transmission intensity of this cell was converted to the voltage signal, which was fed back negatively to keep the transmission proportional to the input signal. Figure 4 (b) shows a block diagram that produces an inverse functional voltage of the capacitance-voltage property. The Wien-bridge oscillator circuit was used to implement the capacitance property into the circuit. The capacitance of the LC cell was used to determine the frequency of the oscillation, and the output voltage by which the LC cell capacitance was varied drove the LC cell so that its frequency was varied. The change of the cell capacitance, that is, the change of the frequency is fed back to control the output voltage by a frequency-voltage conversion circuit which varies in proportion to the input voltage. Thus, the inverse functional property of the capacitance-voltage curve can be obtained. The compensated properties using the guest-host cell and the capacitance of the LC cell are shown in Figs. 5 (a) and (b)

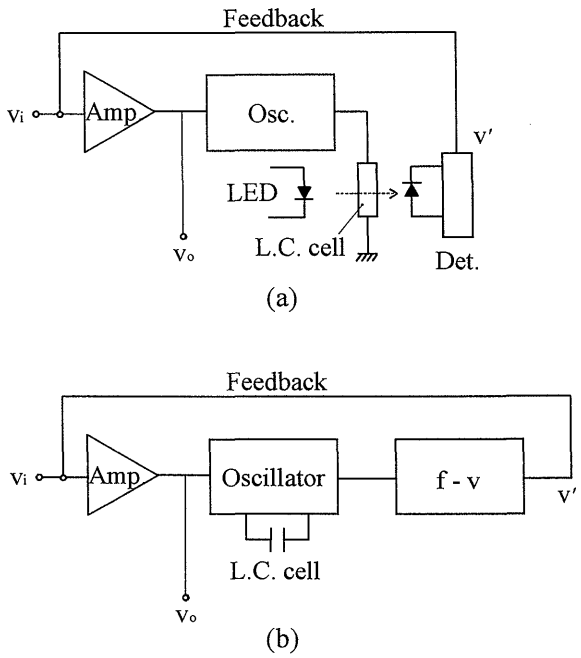

Fig. 4. Block diagrams to produce the compensation driving voltage using (a) guest-host LC cell and (b) capacitance of the LC cell.

for various temperatures, respectively.[14] It is seen that the nonlinear properties can be compensated, and the temperature dependence is also compensated. Using the capacitance properties of the LC lens itself, the nonlinearity of the lens can be compensated, and no LC cell other than the LC lens is necessary.

2.4 *Applications of the LC Lens*

In the early stage of studies on the LC lens, the purpose of the research was to develop convenient eyeglasses with variable focusing properties for persons who had to wear several pairs of glasses because of an eye disease such as cataracts.[15] However, with development of an intraocular lens which is now in wide use, the need for variable focusing glasses has been eliminated. Application of the LC lens to optical testing is described in this review.

Nondestructive optical testing using an interferometer

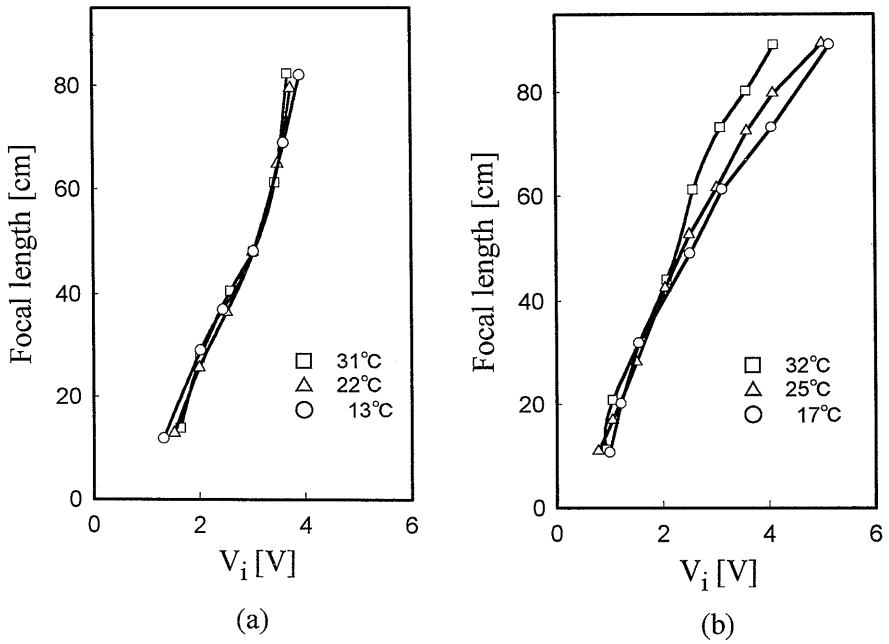

Fig. 5. Compensation properties with (a) guest-host LC cell and (b) homogeneously aligned LC cell.

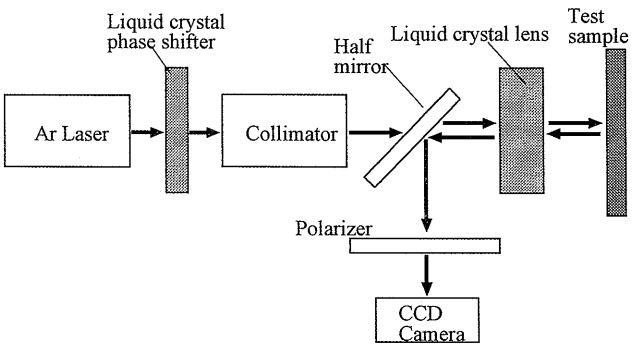

Fig. 6. Common path interferometer system using LC cells.

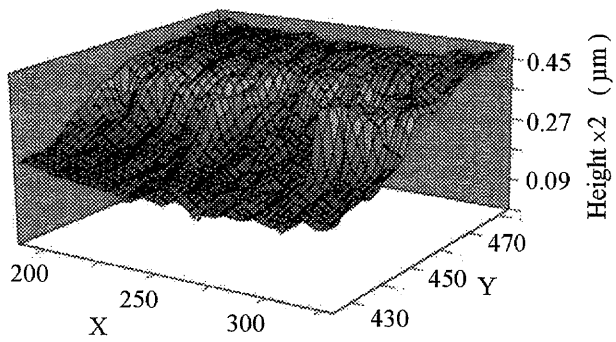

Fig. 7. Three-dimensional plot of the step profile.

is a highly sensitive measuring method, and a common path interferometer is important for a practical testing system, where a birefringent optical component such as a double focusing or a bifocal lens is used as a beam splitter.[16–18] The bifocal lens is made from a large, defect-free optical crystal such as calcite, but is very expensive. The LC lens has bifocal properties and a large aperture lens can easily be fabricated by preparing suitable cell structures. The experimental system of the LC lens interferometer is shown in Fig. 6.[19] The lens was prepared using a plano-concave glass lens (radius of curvature: 26 mm) as a substrate and nematic LC materials (E7) that were selected for refractive index matching between a glass lens and the ordinary index of the materials. The incident ordinary ray passes through the lens without focusing, but the extraordinary ray converges with the focal length of 110 mm. The surface of the test sample is set exactly at the focal point of the extraordinary ray, which is used as a reference beam. The ordinary ray is used as a test beam and has the phase information of the test sample. The interference fringe patterns between the ordinary and extraordinary rays give the wavefront information of the ordinary ray. An Ar laser (488 nm) is used as a light source, and another homogeneously aligned LC cell is used to introduce a 4-step phase shifting in this system. The cross sectional step profile of vacuum deposited Al thin film is shown in Fig. 7[19]; thickness of this film is measured within an accuracy of about $\lambda/10$ in this system.

3. LC Microlens Using Molecular Orientation Effects by a Nonuniform Electric Field

3.1 Molecular Orientation Effects in an Axially Symmetrical Nonuniform Electric Field

As mentioned above, by application of a relatively low and uniform electric field across the plane-paralleled elec-

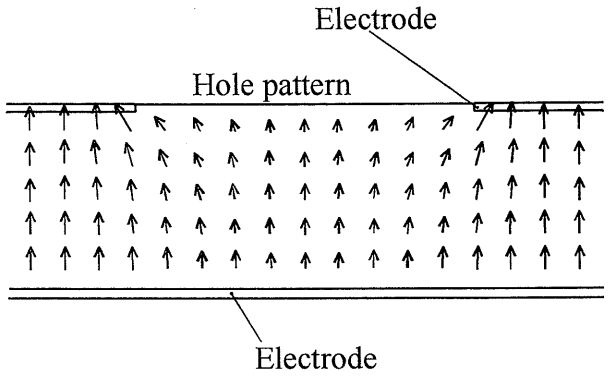

Fig. 8. Cross section of the non-uniform electric field produced by a hole-patterned electrode.

trodes of the LC cells, the director orientation in the cells is easily controlled. The director of the LC can also be reoriented by a non-uniform electric field. For example, an axially symmetrical non-uniform electric field is produced by the structure with a hole-patterned electrode, and a radial distribution of refractive indices; thus a small LC lens (LC microlens) can be obtained by a molecular orientation effect.[9,20] In earlier work, LC cells with asymmetric electrodes were fabricated by using a hole-patterned electrode that was made by photolithographic etching of thin aluminum (Al) films deposited on a glass substrate and an ITO-coated counter electrode.[9,20] Both surfaces of the electrodes were coated with PVA and rubbed to give a homogeneous orientation. A nematic LC with a positive dielectric anisotropy (K15) was put into the cell fabricated from this pair of substrates and the space of suitable thickness. The optical properties of this type LC cell would depend on the director orientation effects resulting from the nonuniform electric field inside the cell. A cross section of the cell along the diameter of the hole-pattern is shown in Fig. 8.[9] The electric field produced by the hole-patterned electrode and a plane electrode is shown as small arrows, where the electric field is calculated by the finite element method. The directions of the arrows show that of the field distribution and the lengths correspond to the field strength. The intensity of the electric field is maximum at the edge of the hole-pattern and grows smaller as it approaches the center. The angle between the direction of the electric field and the perpendicular direction to the substrate is also maximum at the edge of the hole-pattern.

When no electric field is applied, the director is uniformly oriented parallel to the substrate surface, and the refractive index is n_e for the extraordinary ray. The distribution of the refractive index is thus uniform and the LC cell is the same as a transparent flat panel. The director near the edge of the hole-pattern is forced to align along the directions of the electric field when voltage above the threshold is applied across the LC cell. The director near the center of the hole-pattern, however, remains parallel

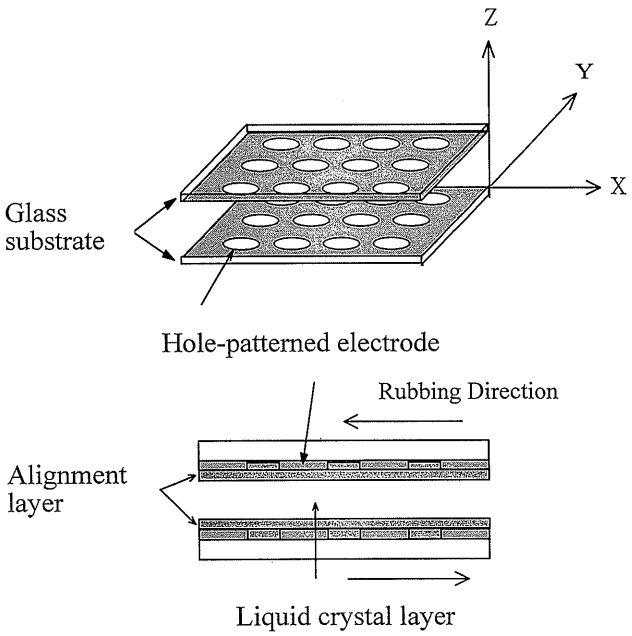

Fig. 9. Structure of the LC microlens.

to the substrate; the refractive index near the edge then is smaller than the value of n_e, does not change near the center and itself becomes n_e. The refractive index gradually changes from the minimum value at the edge of the hole-pattern to the maximum value of n_e at the center in this non-uniform director orientation. The LC cell prepared using the substrates with a hole-patterned electrode is therefore expected to behave like a graded index converging lens. When the applied voltage increases, the gradient of the refractive index becomes less steep and the focal length becomes longer, because the director near the center of the hole-pattern begins to reorient and the refractive index at the center also becomes smaller than n_e. As the applied voltage increases, the focal length becomes longer, and the LC cell changes to a concave (diverging) lens for high voltages.[9,20]

In the LC microlens with the asymmetric electrode structure, however, a disclination line which worsens the lens properties is usually observed in the direction perpendicular to the director of the LC. Generation of such a disclination line is suppressed by adopting a hybrid-aligned molecular orientation,[21,22] but the lens properties are not improved much because the optical lens center of the hybrid-aligned LC microlens tends to shift under application of an electric field.[21] Deteriorating factors such as a disclination line or a shifting effect of the lens center can be eliminated by a homogeneously aligned LC microlens with a symmetric electrode structure of hole-patterned electrodes on both substrates.[23,24]

Figure 9 shows the structure of the LC microlens cell, which is similar to the conventional LC cell except for the circular hole-patterns on both substrates. A hole-patterned electrode was made by photolithographic etching of an Al thin film deposited on a glass substrate. Both

electrode surfaces were coated with PVA and treated by rubbing. For the LC cell two substrates of suitable thickness were assembled, the hole-patterns arranged accurately, and a nematic LC with a positive dielectric anisotropy (K15) was put into the cell.

Figure 10 shows a cross section of the cell along a radius of the hole-pattern and a typical equipotential surface distribution of the nonuniform electric field produced by the symmetrically patterned electrode structure. When the voltage is removed, the director of LC is uniformly parallel to the substrate with a small pretilt angle resulting from the rubbing surface treatment (Fig. 11 (a)), and the refractive index distribution for the extraordinary ray is uniform with the value of n_e. If a voltage which is low but higher than the threshold is applied to the LC cell, spatial tilt angle distribution of the director can be created as shown in Fig. 11 (b). The directors of the LC around the edge of the hole-pattern are forced to tilt according to the pretilt direction and no reversely tilted regions, which lead to a disclination line, are observed. The refractive index around the central part of the hole-pattern where the tilt angle is small, is the largest, and it gradually decreases with distance from the center.

Figures 12 (a) and (b) show the interference fringe patterns of the LC microlens, where the diameter of the hole-pattern is 300 μm and the thickness of the LC (K15) layer is 100 μm with application of 1.88 V and 2.00 V, respectively. Circular fringe patterns appear when voltage is applied to the LC cell. The optical path (retardation) distribution, that is, the gradient-refractive-index distribution, determined from the interference fringe patterns is shown in Fig. 13, where solid lines are quadratic fitting curves. It is seen that nearly parabolic distribution is obtained, and the total number of interference fringes begins to increase and becomes maximum at relatively low applied voltage. Varying the applied voltage can continuously change the parabolic refraction-index distribution properties in the hole-patterned area, therefore, variable-focusing properties can be obtained. Figure 14 shows a

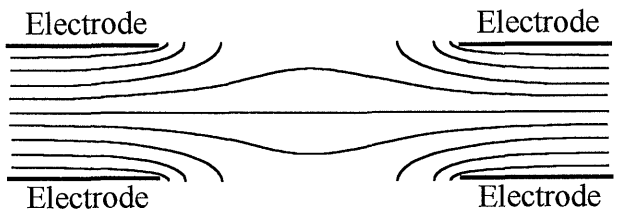

Fig. 10. Potential distribution of the non-uniform electric field.

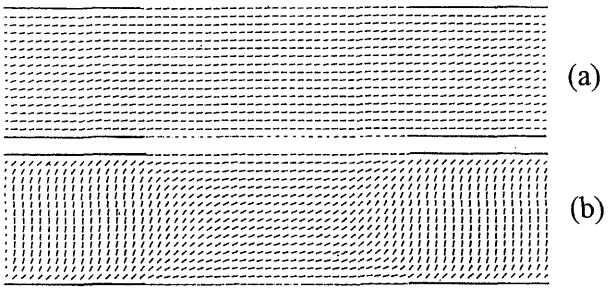

Fig. 11. Director distribution properties for (a) without voltage and (b) $V_{th} \times 3$, where V_{th} is a threshold voltage.

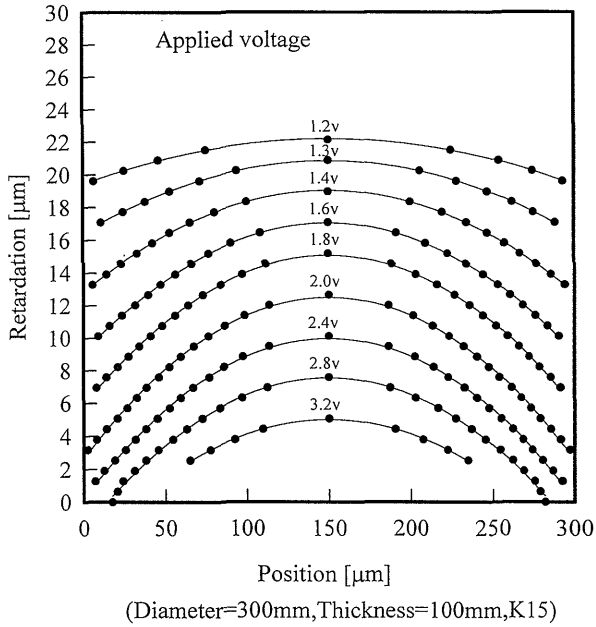

Fig. 13. Distribution properties of the refractive index for an extraordinary ray.

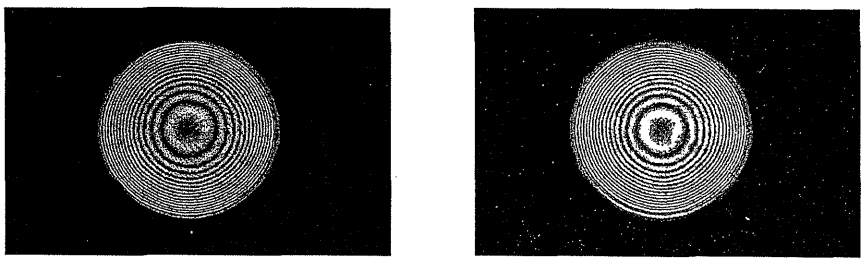

(a) 1.88 V (b) 2.00 V

Fig. 12. Interference fringe patterns of the LC microlens.

typical focusing property of the LC microlens, and a sharp focusing profile of which FWHM (full width at a half-maximum) is about 2 μm is seen. From these results, it is clear that distribution of an optical path in the hole-patterned area becomes axially symmetric like a convex lens and relatively good focusing properties are achievable.

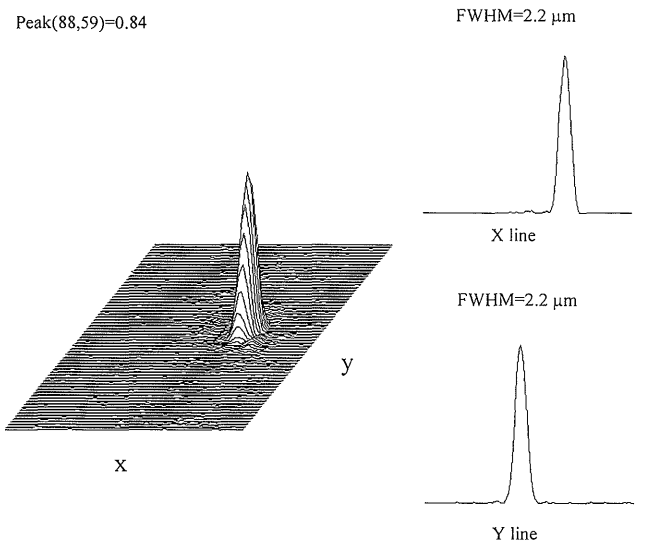

Fig. 14. Light intensity profile at the focal point (D/t=120/40 μm, V=3.0 V).

To improve the optical properties of LC devices, particularly in a case utilizing the inhomogeneous director distribution, investigation of the molecular orientation states in a two- or three-dimensional space is very important. The molecular orientation states in the electric field can be determined using a computer simulation technique.[25,26] The director distributions shown in Fig. 11 were obtained by simulation using the finite element method. However, the molecular orientation states including the disclination line and its structure have not yet been determined.

A technique for visualization of the cholesteric texture was proposed using an LC diacrylate and a scanning electron microscope (SEM).[27] However, it is difficult to determine the distribution state of the continuous molecular orientation in LC devices. Recently, a novel procedure for observation of cross-sectional images of an LC cell and determination of a molecular orientation in the cell has been proposed[28] using UV (ultra-violet) curable LC materials.[29] The UV-curable LC has a nematic phase at room temperature and is characterized by the property

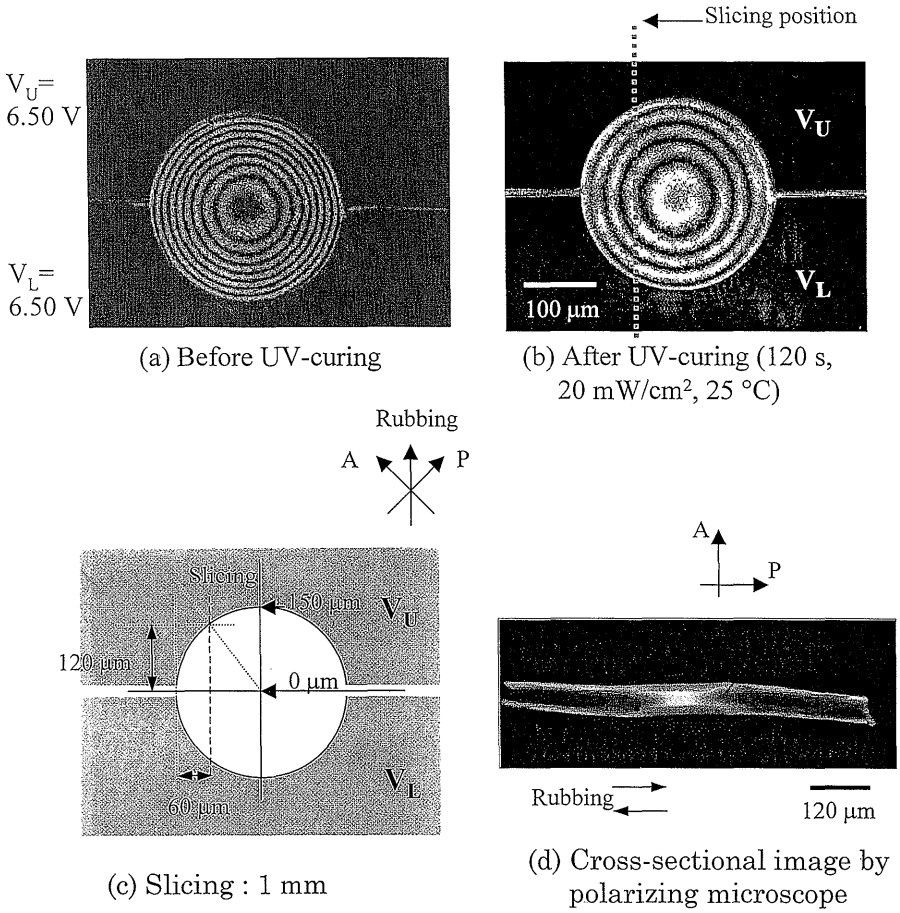

Fig. 15. Interference fringe pattern (a) before UV curing, (b) after curing, (c) thin successive slicing of UV curable LC microlens, (d) cross sectional image of a slice using a polarizing microscope.

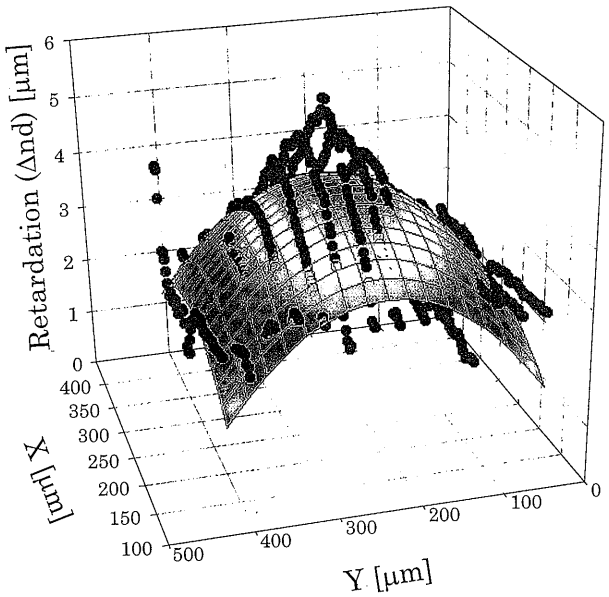

Fig. 16. Three-dimensional refractive distribution profile of LC microlens.

of photoinduced polymerization in the nematic phase.[29] The fabrication process for visualizing the molecular orientation was as follows. LC cells prepared using the UV curable LC (Mixture E: Dainippon Ink and Chemicals Inc.) were irradiated with UV light while appropriate voltage was applied. The cured LC cell was cut into slices and lapped to make a thin sample, allowing the molecular orientation in the cross section of the cell to be visualized by means of the distribution of the transmitted light intensity seen using a polarizing microscope with crossed polarizers. The cross-sectional director distributions in LC cells can also be calculated using absorption of the dichroic dye with the same direction of LC molecules.[30] The structures near the Grandjean lines in the wedge-shaped cholesteric LC cells were clearly visible.[31]

The three-dimensional molecular orientation states in the LC microlens are visualized by the polarization dependence of the transmission light intensity through the very thin successive slices of a UV curable LC microlens,[32] which are prepared using the UV curable LC (Mixture E). The thin successive slices about 1 μm in thickness were made by slicing with a microtome after photopolymerization in this case. Figures 15 (a) and (b) show interference fringes of the LC microlens constructed using the UV curable LC and a pair of substrates with a hole-patterned electrode that is divided into two parts. Structures and properties of the divided-electrode LC microlens are described later in 3.3.2. The fringes observed before UV irradiation are shown in (a). The number of interference fringes in the hole-patterned area decreases while photopolymerization proceeds and the fringe pattern after the photopolymerization is shown in (b), where the total number of interference fringes has decreased to 60%. However, relatively good focusing and imaging properties can be obtained in this microlens even after photopolymerization.[33] The cross-sectional image at the position indicated in (c) is shown in (d). The area where the director of the LC coincides with the polarization direction of the polarizer or analyzer is dark, and the transmittance increases as the angle between the director and the polarizer nears to $\lambda/4$. The director distribution in the cross section of the LC microlens can be estimated and the results are similar to the simulated distributions, for example, as shown in Fig. 11. Three-dimensional refractive index distributions of the LC layer in the LC microlens are estimated using the successive series of thin slices and are shown in Fig. 16 where parabolic surface fitting to the measured values is implemented. Though the coincidence between the fitting surface and the observed values is not completely good around the center area of the LC lens, three-dimensional refractive-index distribution of the LC microlens can be obtained using the distribution of transmission light intensities of the cross-sectionally sliced samples. This technique can be widely applied for analyses of other LC devices with complex molecular orientation profiles.

3.2 Dependence of Optical Properties on the Device and Material Parameters in the LC Microlens

The optical properties of the LC microlens are determined by the spatial distribution of the electric field in the hole-patterned area and material properties of the LCs. That is, they usually depend on the device structure (ratio of the cell thickness t and the diameter of the hole-patterned electrode D),[34] which determines the spatial distribution of the electric field in the LC cell, and the material parameters of elastic constants, dielectric constants and birefringence properties.

First, the D/t values are optimized so that the numerical aperture (NA) of the LC microlens has maximum value. LC microlenses with different D/t values were fabricated using K15 and optical properties were measured. Figure 17 shows the relationship between D/t values and the largest value of NA obtained under optimum driving voltage, since the numerical aperture depends on the applied voltage level.[34] It is seen that the numerical aperture of the LC microlens depends on the D/t values, and the optimum D/t value is about 2–3, where the effective area with the parabolic refractive-index distribution within the hole-patterned area becomes maximum. Thus, the NA can be controlled by setting a device parameters such as the D/t value.

The molecular orientation and the optical properties of the LC devices in an electric field are generally affected by the material constants of LC: elastic constants, dielectric anisotropy $\Delta\varepsilon$ and birefringence Δn. The driving voltage of the LC microlens can be decreased by using LC materials with a large $\Delta\varepsilon$, and the applied voltage at which the numerical aperture of the LC microlens becomes maximum decreases with increasing $\Delta\varepsilon$. The maximum numerical aperture NA_{max} of the LC microlens tends to increase as $\Delta\varepsilon$ increases, and it also increases as Δn increases. However, it is found that LC microlenses

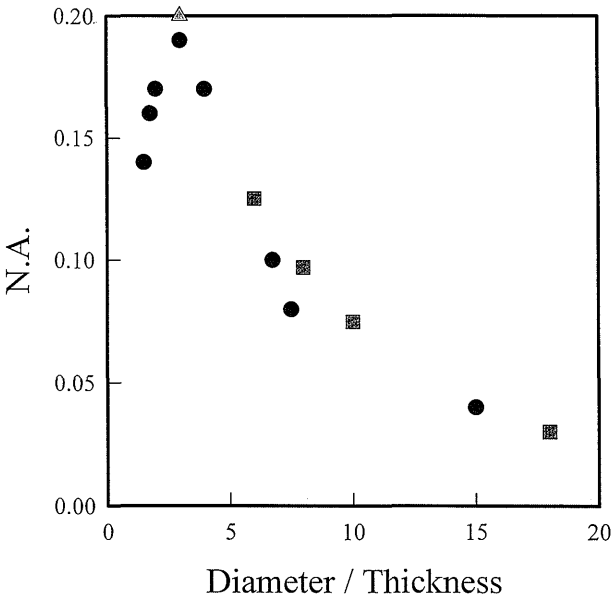

Fig. 17. Relationship between diameter/thickness and NA of the LC microlens. ●, 40 μm; ■, 50 μm; ▲, 100 μm.

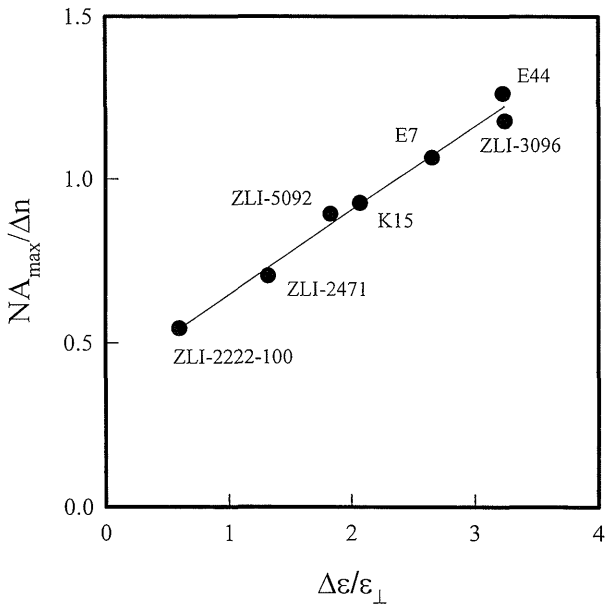

Fig. 18. Relationship between dielectric anisotropy $\Delta\varepsilon$ and NA_{max} of the LC microlens.

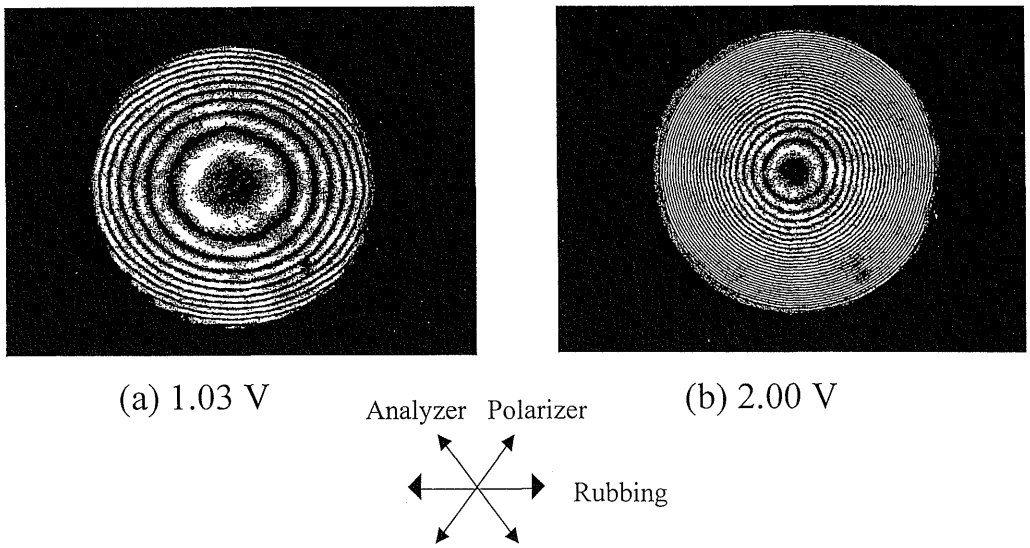

Fig. 19. Interference fringe patterns with various applied voltages.

with nearly the same $\Delta\varepsilon$ or Δn value do not always have a similar NA_{max}.[35] Figure 18 shows the relationship between $\Delta\varepsilon$ and NA_{max} of the LC microlens, where NA_{max} is divided by Δn to normalize the vertical axis in the figure. A linear relationship is obtained between the $NA_{max}/\Delta n$ and the dielectric anisotropy.

Figures 19 (a) and (b) show interference fringe patterns of the LC microlens prepared using K15. The diameter and the cell thickness are 500 μm and 200 μm, respectively. When a relatively low voltage is applied to the LC microlens, the interference fringes are elongated along the rubbing (director) direction although the electrode pattern is exactly circular as shown in (a).[36] It becomes more remarkable in the LC microlens prepared using nematic LC such as E7 (Merck).[35] These microlenses have anisotropic focusing properties, that is, the gradient-refractive-index profile in the rubbing direction is different from that in the direction perpendicular to the rubbing direction. Thus an astigmatic aberration is generated.

When the numerical aperture becomes maximum by control of the applied voltage, the gradient-refractive-index profiles of the LC microlens show nearly parabolic distributions. The anisotropic properties are evaluated in terms of the differences in the coefficients of second-order fitting curves in the directions parallel and perpen-

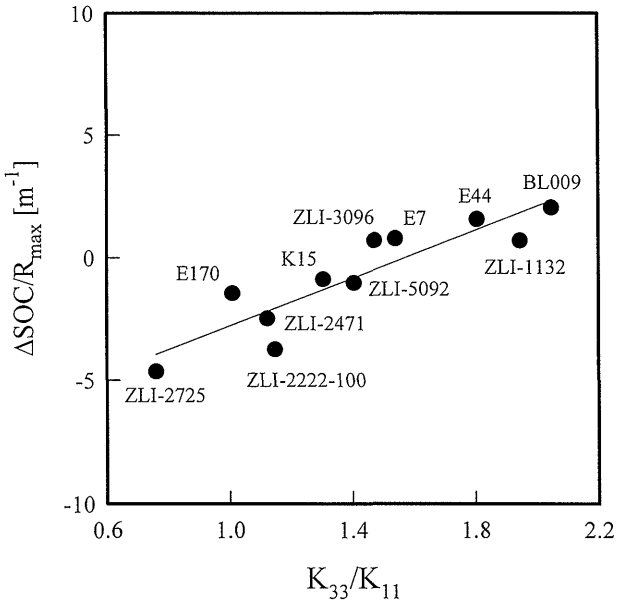

Fig. 20. Dependence of $\Delta SOC/R_{max}$ on elastic constant K_{33}, K_{11}.

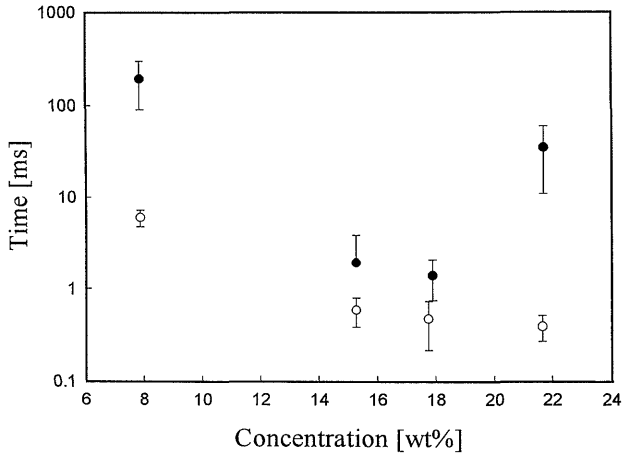

Fig. 21. Response and recovery properties as a function of polymer concentration. ○, response time; ●, recovery time.

dicular to the rubbing direction. That is, the astigmatic aberration is expressed by the difference in the second-order coefficients ΔSOC. The influence of elastic constants on the aberrations of the LC microlens was investigated. Figure 20 shows the relationship between ΔSOC and the elastic constants K_{33}/K_{11}, where R_{max} is defined as the maximum retardation of the gradient-index curves in the rubbing direction.[35] The results suggest that the astigmatic aberration of the LC microlens tends to increase with increasing K_{33}/K_{11}.

The astigmatic aberration also strongly depends on the ellipticity of the hole-pattern[36] and applied voltage level,[35,36] and can be minimized by adjusting the ellipticity and the applied voltage, respectively. Using the experimental results, we were able to obtain good focusing properties and smaller values of FWHM which were less than 1.2 times the value of FWHM of the diffraction limit. In conclusion, an LC material with large dielectric anisotropy and small elastic anisotropy as well as large birefringence is required to fabricate an LC microlens with good optical properties.[36]

3.3 Improvement of the Properties of the LC Microlens

3.3.1 Polymer stabilized LC microlens

The polymer stabilization technique has been extensively investigated in the LC display research field,[37,38] where a small amount of polymer dissolved into the LC forms a polymer network and improves the optical properties of the LC cell. It is found that a small amount of polymer is also effective in suppressing the disclination lines generated in the LC microlens.[39] In addition, the gradient-distribution state of the LC molecules in the LC microlens while applying voltage to the LC cell can be stabilized by the polymer network formed by the UV curable LC, and the focusing property of the LC microlens is maintained without applying voltage.[40] Furthermore, applying voltage after forming the polymer network can alter the focusing property.[40] Although the variable range of focusing is rather limited in the polymer-stabilized LC microlens, this polymer stabilization technique has been confirmed to eliminate the drawback of a conventional LC microlens.[41]

The response and recovery times of voltage application are very important in application of the LC microlens to real time light controlling devices. The ratio of the lens aperture and cell thickness is a very important factor in achieving excellent lens properties as mentioned above. The LC microlens has a very thick LC layer (larger than several tens of microns) compared with a conventional LC display device, consequently its response time is usually longer than a few seconds. The polymer stabilization technique can also be utilized to improve the response and recovery properties in the LC microlens,[41] since the molecular orientation state in the polymer stabilized LC microlens is similar to the bias-voltage applied to the LC cell where the response and recovery times can be reduced.[42] The response and recovery properties of the polymer stabilized LC microlens are shown in Fig. 21 as a function of UV-curable LC concentration.[43] The driving voltage is determined by the value for 0.2 mm focal length change in each LC microlens, and is very high: several hundred volts. Although the variable focusing range is restricted and higher driving voltage is necessary, about millisecond order of response and recovery times can be attained, which are much faster than those of the usual LC microlens without the polymer network.

3.3.2 LC microlens with divided electrode structure

The most remarkable features of the LC microlens with hole-patterned electrodes are their simple device structures and voltage controllable variable focusing properties. If the hole-patterned electrode is divided into parts and each electrode is driven by a different voltage, beam steering and three-dimensional variable focusing properties can be realized.[44,45] We fabricated 2, 4, and 8-

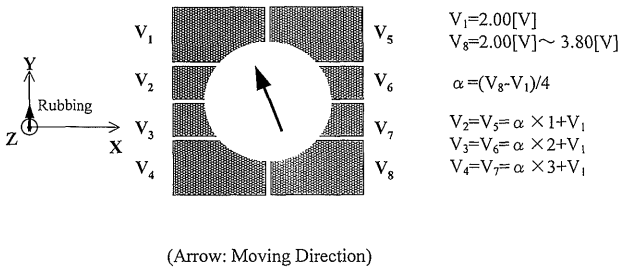

Fig. 22. Divided electrode structures and driving voltage application.

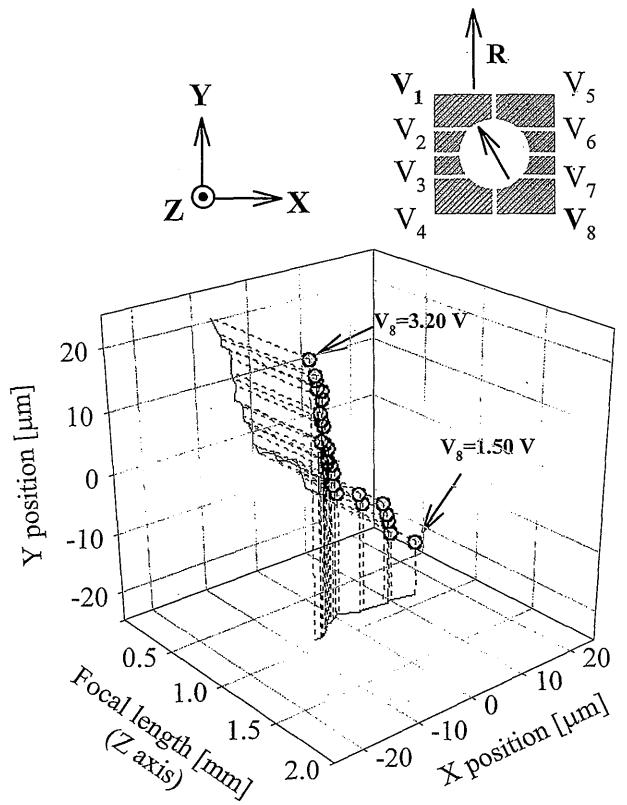

Fig. 23. Beam steering properties of the LC microlens with an 8-divided electrode structure.

divided hole-patterned electrodes using Al thin film deposited substrates and a photolithographic technique. The diameter D of the hole-patterned electrode, which was divided into several regions by slit patterns 10 μm in width, was 300 μm. Each surface of the electrode was coated with PVA and unidirectionally rubbed to produce a homogeneous orientation. The cell thickness t was 100 μm and a nematic LC K15 was used to fill the LC cell. Here the D/t value was determined to be 3, and relatively good focusing properties were obtained. The driving voltages to the LC cell are shown in Fig. 22, where the voltage is linearly distributed to each electrode. An arrow in the figure shows the direction of the beam deflection.

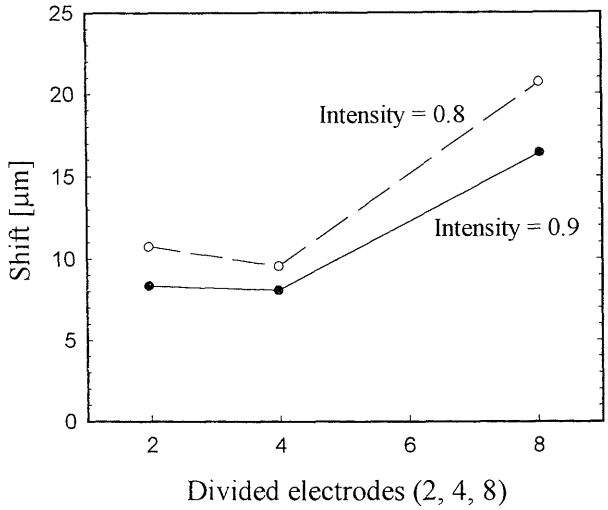

Fig. 24. Relationship between maximum shift of the focal point and number of divided electrodes.

The beam-steering properties of the LC microlens with the 8-divided electrode structure are shown in Fig. 23. Here, the applied voltages are chosen so as not to deform the focusing property and the focusing spot can be controlled in a three-dimensional area. Figure 24 shows the relationship between the maximum shift of the focal point and number of divided electrodes. Parameters are the intensity ratios to the peak value at the focal point when the same voltage is applied to each electrode. It is found that the shift of focusing can be controlled and its range is estimated to be approximately ± 16 μm within the intensity ratios of 90% of the peak values.

As previously mentioned, the fringe patterns of the LC microlenses are elongated along the rubbing direction under a low driving voltage, and this effect induces a large astigmatic aberration.[35] When a higher voltage drives a pair of electrodes along the elongated direction, the distorted fringes tend to be reduced and the astigmatic aberration can be compensated. Tuning the driving voltage to each electrode can also create a suitable astigmatism.[43]

3.4 Applications of LC Microlens

3.4.1 Light scattering properties of LC microlens effects

The focal length of the LC microlens is variable, and is usually so short that strong light scattering properties are obtained. A scattering type display device can thus be attained by fabricating a number of microlenses in a LC cell with an array structure.[46,47] Scattering opaque state and semi-transparent state can be switched by applying or removing the voltage, respectively. The very steep threshold, tunable gray scale and wide viewing angle properties can be obtained in the LC cells with microlens effects as shown in Fig. 25.[46] By arranging the LC microlenses randomly interference effects can be eliminated and the quality of images observed through the semi-transparent LC cell can be greatly improved. The homeotropic-aligned LC microlens array has a polariza-

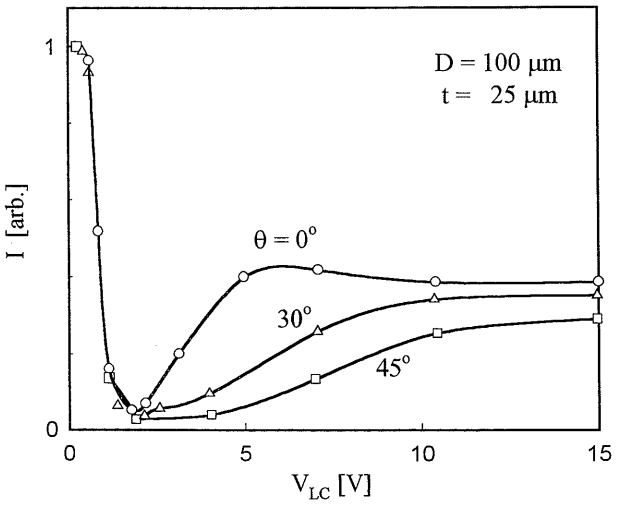

Fig. 25. Transmission light intensity *vs.* applied voltage for various angles of incident light. $\theta=0°$ is normal incidence.

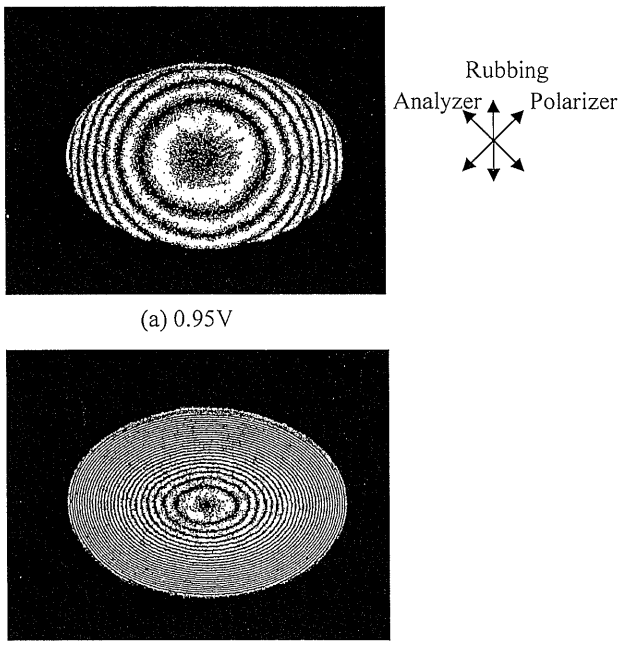

Fig. 26. Interference fringe patterns for various applied voltages. The cell thickness is 200 μm, and the major and minor axes of the elliptical aperture are 400 μm and 600 μm, respectively.

tion independent light scattering effect which extends several micrometers into the infrared wavelength range.[48]

3.4.2 Applications of optical fiber switching and laser diode collimation

As mentioned above, the LC microlens has variable voltage controllable focusing properties, and appears highly promising for applications in optical systems such as optical parallel processing and optical interconnection. For example, the microlens has potential application in an electrically controllable optical fiber coupler or switch.[20,42]

In the field of the optical interconnection, the laser diode (LD) is widely used as a compact light source, however, it has astigmatism and an elliptically distorted beam profile, and undesirably reduces the optical coupling. Various techniques have been proposed to compensate for the astigmatism of the LD beam: the combination of a cylindrical lens and a Selfoc lens,[49] a double wedge anamorphic microlens,[50] and others.[51,52] The anamorphic microlens has great advantages: the astigmatism can be compensated and an elliptically distorted light beam can be converted into a round beam. An anamorphic LC microlens with variable focusing properties was therefore proposed and demonstrated using a pair of elliptically patterned electrodes.[53,54]

The device structure of the anamorphic LC microlens is similar to that shown in Fig. 9, but elliptical hole-patterned electrodes are used. The diameters along the major and minor axes of the elliptical aperture were varied over the range of 200 μm to 600 μm, and the cell thickness was controlled within 200 μm by a spacer. Nematic LC (K15) was injected into the cell and a He-Ne laser (633 nm) was used as a light source. Figures 26 (a) and (b) show typical interference fringe patterns, where the rubbing direction is perpendicular to the major axis of the elliptical aperture.[54] Refractive-index distribution properties of this anamorphic LC microlens are shown in Fig. 27,[54] where the fringes shown in Fig. 26 (b) are elongated along the major axis of the elliptical aperture (perpendicular to the rubbing direction) and the profiles of the refractive-index distribution differ from those in the other axis under higher voltage application. These effects lead to the generation of astigmatism. However, the interference fringe pattern shown in Fig. 26 (a) appears to be nearly circular as a result of cancellation, since it is elongated along the rubbing direction at somewhat above the threshold voltage. The profiles of distribution shown in Fig. 27 are well fitted to parabolic curves at any applied voltage and this anamorphic LC microlens is free from spherical aberration, though there is astigmatism.

An optical setup for collimating the LD beam using the anamorphic LC microlens has been realized in practical applications,. Figure 28 shows the astigmatic beam profile emitted from the LD. This profile is elongated along the direction parallel to the junction (x direction) at the output facet, since the active region of the LD is generally a thin layer. Additionally, the far-field pattern is elongated along the direction perpendicular to the junction (y direction) due to the astigmatism. In this work, the divergence angles of the beam from the LD (635 nm) were reduced by using another lens, since the NA values of the anamorphic LC microlens are at most 0.2 and insufficient. The reduced θ_x and θ_y angles were measured to be 6° and 16°, respectively. Then the anamorphic LC microlens ($D_{\parallel}=400$ μm, $D_{\perp}=600$ μm, $t=200$ μm) was placed in front of the lens and 1.61 V was applied; suc-

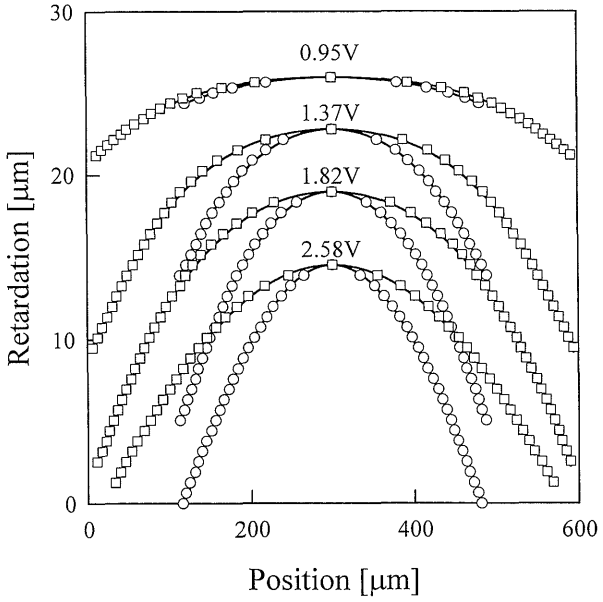

Fig. 27. Refractive index distribution properties of the anamorphic LC microlens for various applied voltages. ○, parallel to the rubbing direction; □, perpendicular to the rubbing direction.

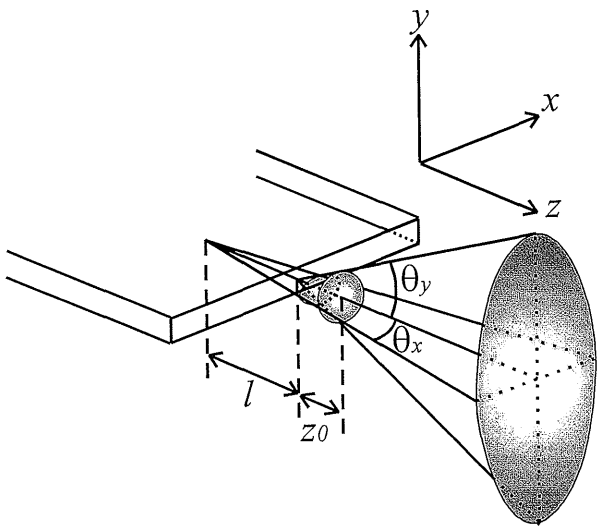

Fig. 28. Astigmatic beam emitted from the laser diode.

cessful compensation for the astigmatism was achieved and nearly round beam profiles can be observed. The divergence of the round beam was measured as 0.4°, which approximately agrees with the calculated value of 0.3°. This confirmed the successful collimation of an LD beam to a round one using the anamorphic LC microlens.[54]

3.4.3 Application to optical haar wavelet transforms with LC elements

Several optical wavelet transform architectures have recently been proposed, and optical filtering systems have been applied to perform wavelet transforms.[55] The

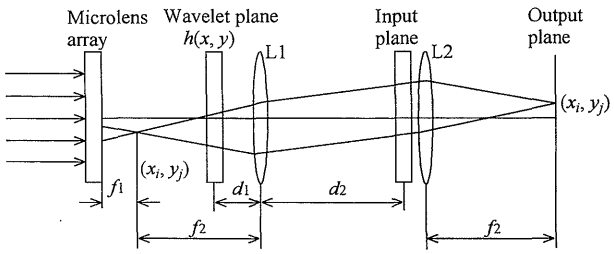

Fig. 29. A shadow-casting system with a microlens array for wavelet transforms.

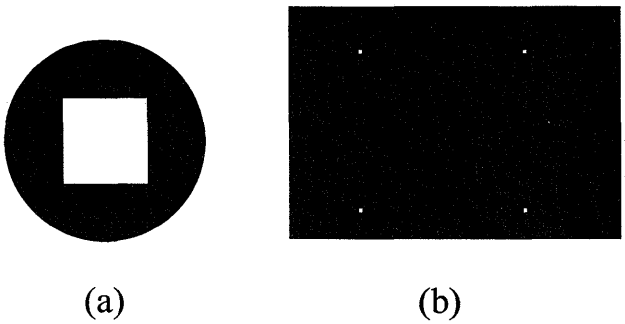

Fig. 30. Haar wavelet transform result of a rectangular pattern. (a) Rectangular pattern. (b) HW transform result of (a).

Haar wavelet is commonly used[56] as the mother wavelet, and its corner mother wavelet and edge mother wavelet are useful for real-time feature extraction. We described the design of Haar wavelet functions by means of zone plates in one- and two-dimensional space domains and then presented a circular Haar wavelet.[57] Optical Haar wavelets can also be generated using patterned LC cells and by adjusting the voltage applied to the LC cell.[58] To implement the optical Haar wavelet transforms using such LC wavelet cells, a shadow-casting system could be set up with a LC microlens array as a spotlight source array.[58] Figure 29 schematically shows the shadow-casting system to implement the wavelet transform.[58] The LC microlens array is located in the front focal plane of lens L_1 and creates a point source array. The light from a particular source point projects the wavelet function, $h(x, y)$, onto the principal plane of L_1. The light beam transmitted through the input plane is then focused at the focal plane of L_2. Nematic LC cells with patterned-electrode structures, where the transparent electrodes are etched into the shapes of one-dimensional, two-dimensional, and circular Haar wavelets, are fabricated to realize the bipolar nature of these wavelets.

A shadow-casting system shown in Fig. 29 was set up with a conventional LC microlens array to perform the Haar wavelet transforms with the LC cell. The diameter of the LC microlens with a symmetrical hole-patterned electrode structure was 400 μm, the pitch of the lens array was 750 μm, and the thickness was 50 μm. A He-Ne laser was used as a light source. The two-dimensional rec-

tangular Haar wavelet transform results of the rectangular pattern are shown in Fig. 30, where the four corners of the pattern are clearly shown.[58] Since the focal length of the LC microlens is variable by controlling the voltage, shadow casting can easily obtain the best Haar wavelet transform results.

4. Summary

A variable focusing LC lens with a lens-shaped LC layer has been fabricated and the focal length can be varied continuously from value for an extraordinary ray to that for an ordinary ray by applying an electric field. Use of a Fresnel-type structure can attain a steep reduction in the response and recovery properties. The nonlinearity of the LC lens for the applied voltage can be compensated using the inverse functional driving voltage that is produced by incorporating the LC cell into the electronic circuit.

The LC lens with variable focusing properties can also be realized using a plane-paralleled structure with a quadratic distribution of refractive index properties, where the LC director is reoriented by an axially symmetric nonuniform electric field produced by a hole-patterned electrode structure. The optical properties of the LC microlens depend on the spatial distribution of the molecular orientation states. The three-dimensional molecular orientation states in the LC microlens can be visualized by the polarization dependence of the transmission light intensity through thin successive slices of a UV cured LC microlens made using UV curable LC materials.

The dependence of optical properties on the device and material parameters in the LC microlens is also discussed. The numerical aperture NA of the LC microlens depends on the ratio of the diameter of hole-pattern D and cell thickness t, and also on the applied voltage level. The optimum value of D/t is about 2–3. The maximum numerical aperture NA_{max} tends to increase as dielectric anisotropy and/or birefringence of LC increase. The astigmatic aberration of the LC microlens depends on the elastic constants (K_{11}, K_{33}) and decreases with decreasing K_{33}/K_{11} and elastic anisotropy.

The polymer stabilization technique that forms the polymer network in the LC layer of the LC microlens can reduce the response and recovery properties. The focusing property is still maintained without applying voltage in the polymer stabilized LC microlens.

Three-dimensional focusing and beam steering functions are attained in the divided electrode LC microlens which has electrodes driven by different voltages. Tuning the driving voltage to each electrode of the LC microlens can compensate the astigmatic aberration, and suitable astigmatism can also be created.

Applications of the LC lenses to optical devices such as a bifocal lens used in a common path interferometer, light scattering display devices, optical fiber switching and LD collimation, and a shadow casting system in optical Haar wavelet transforms are demonstrated. While there may currently be few examples of practical use for the LC lens, further application possibilities in various fields are anticipated.

Acknowledgments

The author would like to acknowledge the cooperation of Dr. T. Nose, Dr. S. Masuda, Ms. R. Yamaguchi, and Mr. M. Honma. Thanks are also due to many students who graduated from his laboratory for their experimental assistance.

References

1) P. J. Collings: *Liquid Crystals* (Princeton University Press, Princeton, 1990) Chap. 1, p. 7.
2) C. Hu, J. R. Whinnery and N. M. Amer: IEEE J. Quantum Electron. **QE-10** (1974) 218.
3) J. P. Sheridan and T. G. Giallorenzi: J. Appl. Phys. **45** (1974) 218.
4) A. P. Fray and D. Jones: Electron. Lett. **11** (1975) 7.
5) S. Sato and A. Kikuchi: OYO BUTURI **45** (1976) 938 (in Japanese).
6) S. Sato: Jpn. J. Appl. Phys. **18** (1979) 677.
7) S. T. Kowel, D. S. Ceverly and P. G. Kornreich: Appl. Opt. **23** (1984) 278.
8) S. Sato: *The World of Liquid Crystals* (Sangyo Tosho Inc., Tokyo, 1994) Chap. 6, p. 177 (in Japanese).
9) T. Nose and S. Sato: Liq. Cryst. **5** (1989) 1425.
10) S. Sato, A. Sugiyama and R. Sato: Jpn. J. Appl. Phys. **24** (1985) L626.
11) S. Sato: OYO BUTURI **63** (1994) 57 (in Japanese).
12) S. Sato, T. Nose, R. Yamaguchi and S. Yanase: Liq. Cryst. **5** (1989) 1435.
13) T. Nose and S. Sato: Electron. Lett. **23** (1987) 878.
14) T. Nose and S. Sato: Trans. IEICE **J72-C** (1989) 619 (in Japanese).
15) F. Sakai, H. Takahashi, H. Uchiyama and S. Sato: J. Ophthalmolog. Opt. Soc. Jpn. **9** (1988) 30 (in Japanese).
16) J. Dyson: J. Opt. Soc. Am. **47** (1957) 386.
17) H. Kikuta, T. Tanabe and K. Iwata: Opt. Rev. **1** (1994) 266.
18) Y. Xiang, C. Xiang and G. Zhang: Opt. Eng. **32** (1993) 1080.
19) T. Nose, S. Masuda and S. Sato: Proc. SPIE **3143** (1997) 165.
20) T. Nose and S. Sato: Proc. SPIE **1230** (1990) 17.
21) T. Nose, S. Masuda and S. Sato: Mol. Cryst. Liq. Cryst. **199** (1991) 27.
22) S. Masuda, T. Nose and S. Sato: Kogaku **20** (1991) 232 (in Japanese).
23) T. Nose, S. Masuda and S. Sato: Jpn. J. Appl. Phys. **30** (1991) L2110.
24) T. Nose, S. Masuda and S. Sato: Jpn. J. Appl. Phys. **31** (1992) 1643.
25) G. Haas, H. Wohler, M. W. Fritsch and D. A. Mlynski: *Proc. 10th Int. Display Research Conf., Berlin, 1990*, p.252.
26) A. Lien: Appl. Phys. Lett. **62** (1993) 1079.
27) I. Hynderickx, D. J. Broer and Y. Tervoort-Engelen: Liq. Cryst. **15** (1993) 745.
28) S. Masuda, T. Nose and S. Sato: Jpn. J. Appl. Phys. **34** (1995) L1055.
29) H. Hasebe, K. Takeuchi and H. Takatsu: *Proc. 14th Int. Display Res. Conf., Monterey, 1994*, p. 161.
30) S. Masuda, S. Fujioka, T. Nose and S. Sato: Mol. Cryst. Liq. Cryst. **303** (1997) 231.
31) S. Masuda, T. Nose and S. Sato: Liq. Cryst. **20** (1996) 577.
32) S. Takahashi, S. Masuda, S. Yanase, T. Nose and S. Sato: *Tech. Rep. IEICE OME98-112, 1998*, p.59.
33) S. Masuda, T. Nose and S. Sato: Appl. Opt. **37** (1998) 2067.
34) S. Masuda, S. Fujioka, M. Honma, T. Nose and S. Sato: Jpn. J. Appl. Phys. **35** (1996) 4668.
35) S. Masuda, M. Honma, T. Nose and S. Sato: Jpn. J. Appl.

Phys. **36** (1997) 2765.
36) M. Honma, T. Nose and S. Sato: Opt. Rev. **6** (1999) 139.
37) D. K. Yang and J. W. Doane: *Proc. SID Int. Symp. 1992*, p.759.
38) H. Hasebe, H. Takatsu, Y. Iimura and S. Kobayashi: Jpn. J. Appl. Phys. **33** (1994) 6245.
39) T. Nose, S. Masuda, S. Sato, J. Li, L. C. Chien and P. J. Bos: Opt. Lett. **22** (1997) 351.
40) S. Masuda, T. Nose and S. Sato: Jpn. J. Appl. Phys. **37** (1998) L1251.
41) H. Kusanagi, S. Masuda, T. Nose and S. Sato: Mater. Sci. Forum **308–311** (1999) 591.
42) T. Nose and S. Sato: Trans. IEICE **75-C-I** (1992) 155 (in Japanese).
43) S. Sato and T. Nose: Proc. SPIE **3800** (1999).
44) S. Masuda, H. Ito, T. Nose and S. Sato: *Tech. Digest of 1996 Int. Topical Meeting on Photonics in Switching, Yokohama, 1996*, p. 114.
45) S. Masuda, S. Takahashi, T. Nose, S. Sato and H. Ito: Appl. Opt. **36** (1997) 4772.
46) T. Nose and S. Sato: Proc. SID **32/3** (1991) 177.
47) T. Nose and S. Sato: J. Inst. Television Eng. **47** (1993) 88 (in Japanese).
48) T. Nose, A. Saito and S. Sato: *2nd Korea-Japan Joint Symposium on Information Display EID91–63, Sendai, 1991*, p. 25.
49) Y. Odagiri, M. Shikada and K. Kobayashi: Electron. Lett. **13** (1977) 395.
50) R. A. Modavis and T. W. Webb: IEEE Photon. Technol. Lett. **7** (1995) 798.
51) Z. L. Liau, J. N. Walpole, J. C. Livas, E. S. Kintzer, D. E. Mull, L. J. Missaggia and W. F. DiNatale: IEEE Photon. Thechnol. Lett. **7** (1995) 1315.
52) Z. L. Liau, J. N. Walpole, D. E. Mull, C. L. Dennis and L. J. Missaggia: Appl. Phys. Lett. **64** (1994) 3368.
53) M. Honma, S. Masuda, T. Nose and S. Sato: Proc. SPIE **3143** (1997) 208.
54) M. Honma, T. Nose and S. Sato: Jpn. J. Appl. Phys. **38** (1999) 89.
55) Y. Zhang, Y. Li, E. G. Kanterakis, A. Kats, X. J. Lu, R. Tolimieri and N. P. Caviris: Opt. Lett. **17** (1992) 210.
56) X. Yang, H. H. Szu, Y. Sheng and H. J. Caulfield: Opt. Eng. **31** (1992) 1846.
57) Z. He and S. Sato: Opt. Lett. **19** (1994) 686.
58) Z. He, M. Honma, S. Masuda, T. Nose and S. Sato: Jpn. J. Appl. Phys. **34** (1995) 6433.